LETTER

doi:10.1038/nature11919

MicroRNA-34a regulates cardiac ageing and function

Reinier A. Boon[1]*, Kazuma Iekushi[1]*, Stefanie Lechner[2], Timon Seeger[1,3], Ariane Fischer[1], Susanne Heydt[1], David Kaluza[1], Karine Tréguer[1], Guillaume Carmona[1], Angelika Bonauer[1], Anton J. G. Horrevoets[4], Nathalie Didier[5], Zenawit Girmatsion[3], Peter Biliczki[3], Joachim R. Ehrlich[3], Hugo A. Katus[6,7], Oliver J. Müller[6,7], Michael Potente[1,3]†, Andreas M. Zeiher[3,7], Heiko Hermeking[2] & Stefanie Dimmeler[1,7]

Ageing is the predominant risk factor for cardiovascular diseases[1] and contributes to a significantly worse outcome in patients with acute myocardial infarction[2]. MicroRNAs (miRNAs) have emerged as crucial regulators of cardiovascular function and some miRNAs have key roles in ageing[3,4]. We propose that altered expression of miRNAs in the heart during ageing contributes to the age-dependent decline in cardiac function. Here we show that miR-34a is induced in the ageing heart and that *in vivo* silencing or genetic deletion of miR-34a reduces age-associated cardiomyocyte cell death. Moreover, miR-34a inhibition reduces cell death and fibrosis following acute myocardial infarction and improves recovery of myocardial function. Mechanistically, we identified PNUTS (also known as PPP1R10) as a novel direct miR-34a target, which reduces telomere shortening, DNA damage responses and cardiomyocyte apoptosis, and improves functional recovery after acute myocardial infarction. Together, these results identify age-induced expression of miR-34a and inhibition of its target PNUTS as a key mechanism that regulates cardiac contractile function during ageing and after acute myocardial infarction, by inducing DNA damage responses and telomere attrition.

To study the ageing process in the heart, we compared aged mice (18–20 months old) with young mice (6–8 weeks old). As expected, hearts of aged mice showed increased fibrosis (Fig. 1a), hypertrophy (Supplementary Fig. 2a), shorter telomeres (Fig. 1b) and increased cardiomyocyte apoptosis (Fig. 1c). Expression profiling of miRNAs isolated from the hearts of young and aged mice identified a number of dysregulated miRNAs that are known to have a role in cardiac (patho)physiology and in senescence (Fig. 1d and Supplementary Tables 1 and 2). For example, miR-21 and miR-574-5p are induced in the failing heart[5,6], and miR-146a (ref. 7) and miR-29 (ref. 8) increase during senescence, whereas other previously described age-associated miRNAs were not regulated[9]. Interestingly, the entire miR-34 family (comprising miR-34a, b and c) (Fig. 1e) was significantly upregulated in aged hearts, whereas several cell-type enriched miRNAs were unchanged (Supplementary Fig. 2b). Furthermore, miR-34a levels, but not levels of the muscle-enriched miR-1 and miR-133, also significantly correlated with age in human heart biopsies ($n = 21$), whereas levels of cardiac-enriched miR-208 declined (Fig. 1f, Supplementary Fig. 2c). As miR-34 is involved in apoptosis and senescence[7,10,11], we focused on this miRNA family.

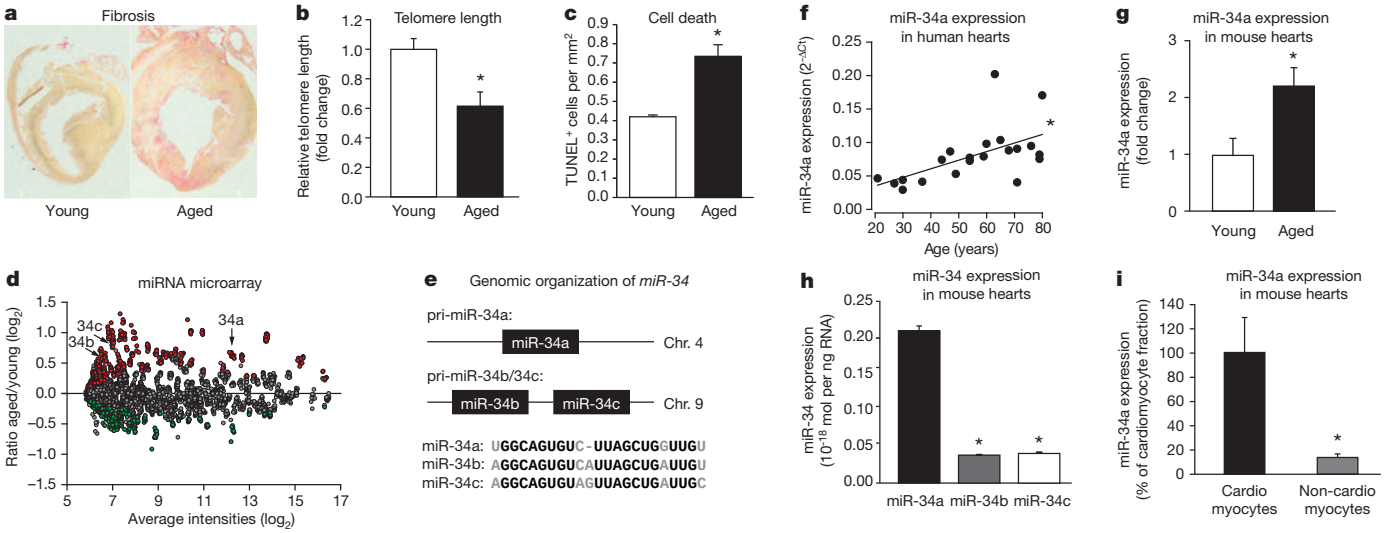

Figure 1 | Ageing induces cardiac miR-34 expression. **a**, Fibrosis staining of hearts from young (6–8 weeks old) and aged (18–20 months old) C57/Bl6 mice. **b**, **c**, Real-time PCR-based telomere length measurement of young and aged hearts (**b**) and cell death quantification using terminal deoxynucleotidyl transferase dUTP nick end labelling (TUNEL) (**c**). **d**, Microarray profiling results of miRNAs in aged and young hearts. **e**, Schematic representation of the primary transcripts encoding miR-34a, b, c, chromosomal location and sequence homologies in mouse. **f**, RNA was isolated from human atrium biopsies and miR-34a expression was measured by real-time PCR. **g**, Real-time PCR expression analysis of miR-34a in aged and young mice hearts. **h**, Quantitative real-time PCR for miR-34a, b and c on RNA from total young mouse heart. **i**, Young heart cell-types were separated using Langendorff-perfusion digestion and miR-34a levels were measured by real-time PCR. $n \geq 3$ for all experiments, $^*P < 0.05$. Error bars depict s.e.m.

[1]Institute for Cardiovascular Regeneration, Centre of Molecular Medicine, Goethe University Frankfurt, 60590 Frankfurt, Germany. [2]Experimental and Molecular Pathology, Institute of Pathology, Ludwig-Maximilians-Universität München, 80337 Munich, Germany. [3]Department of Cardiology, Internal Medicine III, Goethe University, 60590 Frankfurt, Germany. [4]Department of Molecular Cell Biology and Immunology, VU University Medical Center, 1081BT Amsterdam, the Netherlands. [5]Myology Group, UMR S787 INSERM, Université Pierre et Marie Curie Paris VI, Institut de Myologie, Pitie-Salpétrière, Paris Cedex, France. [6]Internal Medicine III, Heidelberg Universiy Hospital, 69120 Heidelberg, Germany. [7]German Center for Cardiovascular Research DZHK, 13347 Berlin, Germany. †Present address: Max-Planck-Institute for Heart and Lung Reseach, 61231 Bad Nauheim, Germany.
*These authors contributed equally to this work.

©2013 Macmillan Publishers Limited. All rights reserved

Quantitative real-time polymerase chain reaction (PCR) confirmed the upregulation of miR-34a in aged mice (Fig. 1g) and showed that miR-34a is the predominantly expressed miR-34 family member in the heart (Fig. 1h). Moreover, miR-34a levels were higher in isolated cardiomyocytes compared to non-cardiomyocytes (Fig. 1i). These data were further corroborated by miR-34a *in situ* hybridization in mouse heart sections (Supplementary Fig. 3).

As miR-34a has been shown to induce apoptosis in cancer cell lines[11] and apoptosis is a fundamental feature of ageing cardiomyocytes (Fig. 1c), we next assessed whether miR-34a has a role in cardiomyocyte apoptosis. Inhibition of miR-34a in rat neonatal cardiomyocytes reduced H_2O_2-induced apoptosis, whereas pre-miR-34a overexpression augmented this apoptosis (Supplementary Fig. 4). To study the role of miR-34a in apoptosis *in vivo*, we inhibited miR-34a by antisense oligonucleotides (antagomirs; Ant-34a)[12], which reduced cardiac expression of miR-34a (Supplementary Fig. 5). To investigate whether miR-34a contributes to age-associated cell death in the heart, we treated 18-month-old mice with 8 mg kg^{-1} Ant-34a, collected the hearts after 1 week and histologically quantified dead cells. Ant-34a treatment reduced the number of dead cells compared to controls (Fig. 2a). To further establish a role for miR-34a in cardiac ageing, we analysed cardiac contractile function by echocardiography in aged (73–83 weeks old) *miR-34a* knockout (*miR-34a*$^{-/-}$) mice (Fig. 2b). Whereas cardiac function in young *miR-34a*$^{-/-}$ mice was comparable to wild-type littermates (Supplementary Fig. 6), the age-associated decline in cardiac function observed in the wild-type mice was prevented in *miR-34a*$^{-/-}$ mice (Fig. 2b). Furthermore, aged *miR-34a*$^{-/-}$ mice hearts were less hypertrophic and showed less cell death, compared to wild-type controls (Fig. 2c and Supplementary Fig. 6). To further substantiate a role of miR-34a in cardiac ageing phenotypes, we analysed *Ku80*$^{-/-}$ mice (*Ku80* is also known as *Xrcc5*), a genetic mouse model of accelerated ageing. In *Ku80*$^{-/-}$ mice cardiac miR-34a levels increased and pharmacological inhibition of miR-34a by locked nucleic acid (LNA)-based antimiRs abolished deterioration of cardiac contractile function (Fig. 2d and Supplementary Fig. 7).

Because apoptosis and fibrosis are also hallmarks after an acute myocardial infarction (AMI) and age aggravates cardiac dysfunction after AMI, we next assessed the role of miR-34a in a mouse model of AMI. miR-34a expression was significantly upregulated in the border zone of the myocardial infarction (Fig. 2e). To test whether miR-34a contributes to cardiac dysfunction after AMI, we induced AMI in mice and injected antagomirs or LNA-based antimiRs. Whereas the extent of myocardial infarction was similar at day 0, cardiac contractile function at two weeks after myocardial infarction was significantly better in antagomir Ant-34a or LNA-based antimiRs treated mice compared to controls, as measured by wall motion score index and ejection fraction (Fig. 2f and Supplementary Fig. 8). These findings were confirmed by analysis of cell death and fibrosis on histological sections of the hearts (Fig. 2g–i).The reduction in the number of dead cells was not confined to cardiomyocytes, but also included non-cardiomyocytes (Supplementary Fig. 9). miR-34a was previously shown to induce senescence in endothelial cells[13] and to inhibit pro-angiogenic cell functions[14,15]. Therefore, we also investigated a potential impact of miR-34a inhibition on neovascularization. Indeed, Ant-34a treatment increased capillary density in the border zone of the infarct *in vivo* and miR-34a modulated angiogenic sprouting of human umbilical vein endothelial cells (HUVECs) *in vitro* (Supplementary Fig. 10). These findings indicate that miR-34a inhibition does not only improve cardiomyocyte survival but also has favourable effects on other cell types present in the heart, for example, endothelial cells.

To identify putative target messenger RNAs of miR-34a, we used three microRNA target prediction tools, miRanda, PicTar and Targetscan 5.1 (Supplementary Fig. 11a). The 49 targets, that were predicted by all three algorithms (Supplementary Table 3), were then compared to genes that were downregulated in aged mice (< 1.5-fold), as assessed in genome-wide mRNA expression profiles of aged and

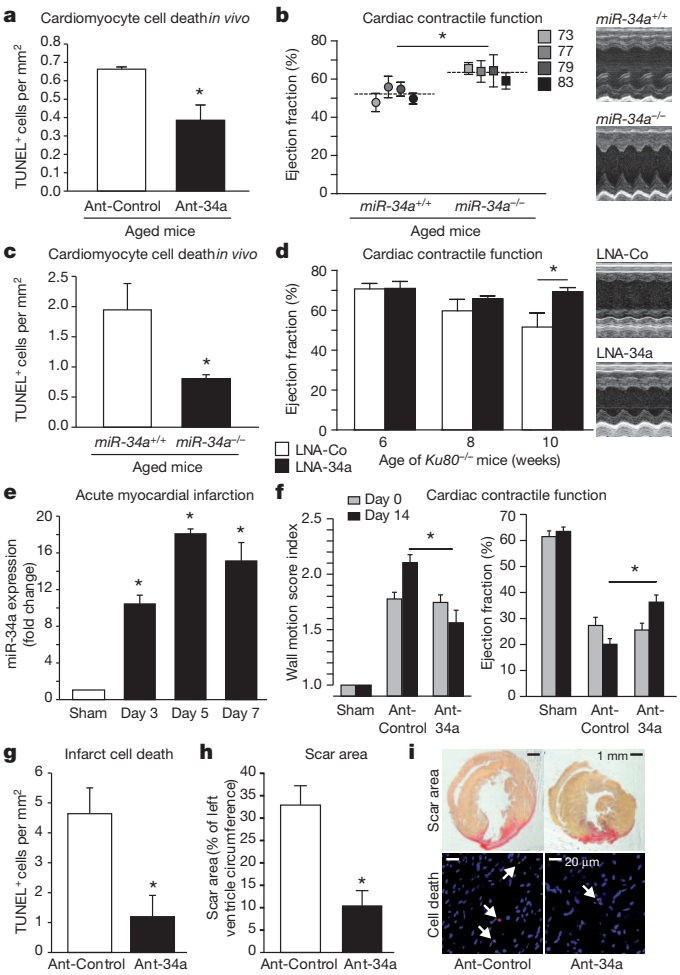

Figure 2 | miR-34a reduction inhibits age-related and myocardial infarction-induced cardiomyocyte cell death and cardiac function. **a**, Cardiomyocyte cell death in aged mice (18 months old) treated with antagomir-34a or scrambled control antagomir. **b**, Echocardiography of *miR-34a*$^{-/-}$ mice and *miR-34*$^{+/+}$ littermates at 73, 77, 79 and 83 weeks of age. Representative m-mode echocardiography images on the right. **c**, Cell death in hearts of *miR-34a*$^{-/-}$ and wild-type littermates **d**, Echocardiography in *Ku80*$^{-/-}$ mice at 6, 8, and 10 weeks of age that received scrambled control locked nucleic acid modified antimiRs (LNA-Co) and LNA-34a weekly subcutaneous from 4 weeks of age. Representative m-mode echocardiography images on the right. **e**, RNA was isolated from the border zone of the myocardial infarction at 3, 5 and 7 days after AMI (black bars) or from sham-operated animals (white bar). miR-34a levels were measured by real-time PCR. **f**, Echocardiography of mice subjected to AMI (day 0). After AMI, mice received control antagomir or antagomir-34a. Echocardiographic data are presented as wall motion score index and ejection fraction. **g**, **h**, Histological sections of infarcted hearts four weeks after AMI were analysed for TUNEL-positive cells (**g**) and scar area (**h**). **i**, Representative scar area and TUNEL stainings. White arrows indicate TUNEL-positive cells. $n \geq 4$ per group for all experiments, $^*P < 0.05$. Error bars depict s.e.m.

young mice (Supplementary Table 4). Only one gene was both a predicted target of miR-34a and downregulated by age on the mRNA level, *Ppp1r10* (also known as *Pnuts*; Supplementary Fig. 11b). In line with the post-transcriptional mechanism of action of miRNAs, PNUTS was even more profoundly downregulated at the protein level in aged hearts (Fig. 3a). PNUTS has a role in apoptosis of cancer cell lines[16], interacts with the telomere regulator TRF2[17], and is involved in DNA repair[18], indicating a potential role in ageing. To assess whether PNUTS is a direct target of miR-34a, we generated luciferase reporter constructs, in which the miR-34a seed target or the PNUTS 3′ untranslated region (3′UTR) is placed behind the luciferase gene. miR-34a inhibited luciferase activity, whereas no effect was observed when the

©2013 Macmillan Publishers Limited. All rights reserved

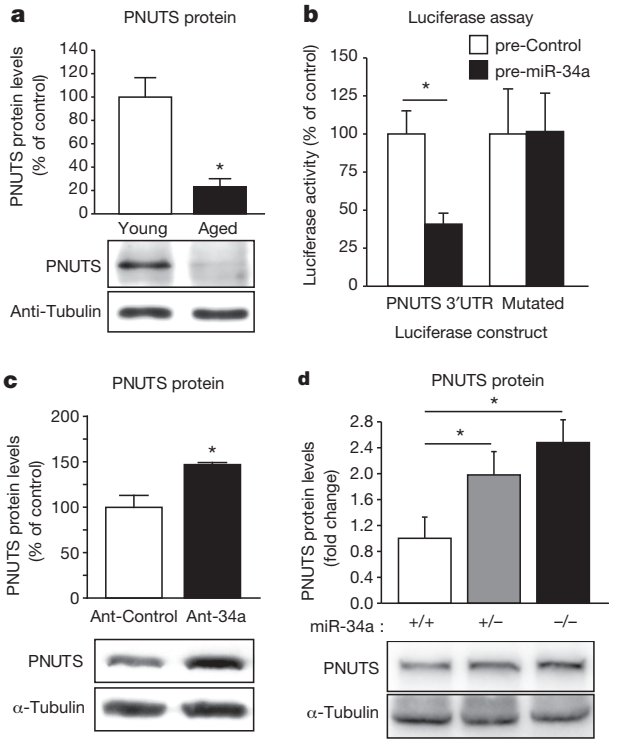

Figure 3 | miR-34a directly targets PNUTS. **a**, Western blot for PNUTS protein in aged (18–20 months) and young (6–8 weeks) mice hearts. **b**, Luciferase assay with wild-type PNUTS 3′UTR or PNUTS 3′UTR mutated in the predicted binding site of miR-34a, transfected with pre-miR-34a or control RNA. **c**, Mice were injected with antagomir-34a or control antagomir. Hearts were collected after 6 weeks and PNUTS protein levels were measured by western blot. **d**, PNUTS levels were measured by western blot in hearts of 19–21-week-old *miR-34a*$^{+/+}$, *miR-34a*$^{+/-}$ and *miR-34a*$^{-/-}$ mice. $n \geq 3$ for all experiments, $^{*}P < 0.05$. Error bars depict s.e.m.

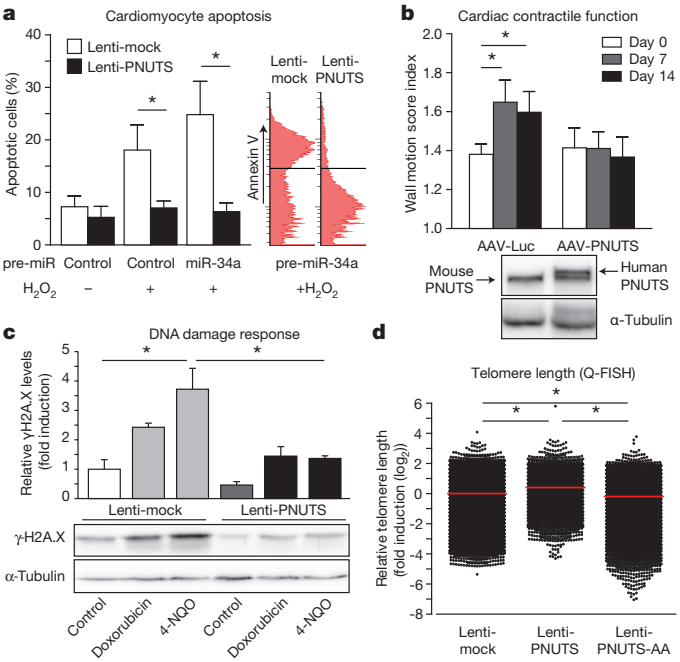

Figure 4 | PNUTS inhibits apoptosis, telomere attrition and DNA damage response in cardiomyocytes. **a**, Cardiomyocytes were transduced with mock or PNUTS overexpression lentivirus and, after 3 days, were transfected with pre-miR-34a or control RNA. Apoptosis was stimulated with 100 μM H_2O_2 on day 4 and quantified by flow cytometry on day 5. Histograms on the right represent total annexin V signal. **b**, Mice received adeno-associated virus (AAV9) to overexpress human PNUTS (AAV-PNUTS) or firefly luciferase (AAV-Luc) under the control of a cardiac-specific promoter 12–14 days before AMI. Heart function was assessed directly after AMI, after 7 and 14 days by echocardiography. PNUTS protein levels were assessed in hearts at 15 days after AMI. **c**, Cardiomyocytes were transduced with mock or PNUTS overexpression lentivirus and treated with doxorubicin (0.1 μM) or 4-nitroquinoline 1-oxide (1 μM) for 24 h or left untreated. γ-H2A.X and α-tubulin were detected by western blot. **d**, Telomere length was assessed in human cardiomyocytes by quantitative fluorescent *in situ* hybridization at 6 days after lentiviral transduction with mock, PNUTS, or mutant PNUTS virus, lacking TRF2 binding capacity (PNUTS-AA). Red line depicts average telomere length per group. $n \geq 3$ for all experiments, $^{*}P < 0.05$. Error bars depict s.e.m.

miR-34a target site was mutated (Fig. 3b and Supplementary Fig. 11). Conversely, inhibition of miR-34a induced luciferase activity (Supplementary Fig. 11c). A reverse-transcriptase-based assay confirmed that miR-34a also binds to the PNUTS 3′UTR (Supplementary Fig. 11e). *In vivo*, Ant-34a-mediated inhibition of miR-34a upregulated PNUTS in the heart (Fig. 3c) and genetic deletion of miR-34a also dose-dependently increased cardiac PNUTS levels (Fig. 3d). Together, these results demonstrate that miR-34a directly targets PNUTS.

Then, we determined whether PNUTS inhibits apoptosis of cardiomyocytes. In PNUTS-overexpressing cardiomyocytes, H_2O_2-induced apoptosis was significantly lower and the miR-34a-mediated enhancement of apoptosis was completely abrogated (Fig. 4a). To assess if PNUTS can also prevent cardiac contractile impairment *in vivo*, we generated adeno-associated virus (AAV9) to overexpress PNUTS under control of a cytomegalovirus-enhanced myosin light chain cardiac promoter (Fig. 4b and Supplementary Fig. 12). Cardiac PNUTS overexpression prevented the deterioration of cardiac contractile function after AMI in mice (Fig. 4b). PNUTS is known to interact with TRF2, and together these proteins have been described to play a role in DNA damage responses (DDR)[18,19]. DNA damage responses can be activated by bona fide DNA damage or by telomere dysfunction, when telomeres are aberrantly recognized as DNA damage, culminating in phosphorylation of CHK2 and apoptosis. Both telomere attrition and defects in DNA repair can cause cardiac dysfunction and cardiomyocyte apoptosis[20–22]. To assess whether inhibition of DNA damage responses could be a possible mechanism for the anti-apoptotic effects of PNUTS, we analysed phosphorylation of CHK2. CHK2 phosphorylation was diminished after ectopic expression of PNUTS in cardiomyocytes (Supplementary Fig. 13). Downregulation of TRF2 using specific small interfering RNAs showed that inhibition of CHK2 activation by PNUTS does not occur in the absence of TRF2 (Supplementary Fig. 13). As DNA damage responses can be caused by DNA damage as well as telomere dysfunction, we assessed the DNA damage marker γH2A.X and telomere length in cardiomyocytes. PNUTS reduced DNA damage in cardiomyocytes, as measured by γ-H2A.X levels (Fig. 4c) and, consistently, inhibition of miR-34a also reduced cardiac DNA damage after AMI (Supplementary Fig. 14). Furthermore, PNUTS overexpression, but not TRF2-binding-deficient PNUTS, reduced telomere attrition *in vitro*, without affecting telomerase activity (Fig. 4d and Supplementary Fig. 15). Together these data show that PNUTS inhibits DNA damage response signalling and prevents AMI-induced cardiac contractile dysfunction, whereas deciphering its function during ageing deserves further studies.

In conclusion, our data demonstrate that inhibition of miR-34a reduces age-induced cardiac cell death and functional decline *in vivo*. Moreover, miR-34a is induced after acute myocardial infarction and inhibition of miR-34a enhances cardiac contractile recovery after acute myocardial infarction. miR-34a suppresses the expression of PNUTS, which inhibits telomere erosion, DNA damage response and apoptosis, thus providing a rationale for the pro-apoptotic effects of miR-34a in cardiomyocytes. In addition to PNUTS, miR-34a has other targets, such as SIRT1 (ref. 23), that confers protection against ischaemia reperfusion injury in the heart (Supplementary Fig. 16)[24]. Nevertheless, we demonstrate that the miR-34a–PNUTS axis has

©2013 Macmillan Publishers Limited. All rights reserved

profound effects on cardiac apoptosis, indicating that PNUTS is a key downstream effector of miR-34a. Moreover, our findings that PNUTS is reduced in ageing and regulates telomere maintenance and DNA damage responses provide a plausible mechanism, by which telomeres erode during ageing. Other targets of miR-34a[25] and functions in non-cardiomyocytes[15] could likewise contribute to its detrimental role in cardiac ageing and dysfunction. Finally, our results identify inhibition of miR-34a as a potential therapeutic strategy to improve cardiac contractile function after acute myocardial infarction.

METHODS SUMMARY

Laboratory animals, ethics and acute myocardial infarction model. Male C57BL/6 mice were obtained from Charles River and Janvier. The animal experiments were approved by the Regional Board of the State of Hessen, Germany. Patient material was obtained under informed consent and according to the declaration of Helsinki. Acute myocardial infarction operations were performed as described[26].

RNA isolation, real-time PCR and transcriptional profiling. Total RNA was isolated with miRNeasy kits from Qiagen and real-time PCR with Applied Biosystems microRNA assays run on an Applied Biosystems StepOnePlus. Quantification of real-time PCR was performed using synthetic microRNA sequences in a calibration curve. Transcriptional profiling was performed by DNAvision on the Agilent-v1 platform (570 miRNAs) or on the Affymetrix 430 v2.0 platform (mRNA, full genome).

Statistical analysis. Data were analysed with GraphPad Prism 5 using student's *t*-tests when comparing two conditions, or with an analysis of variance (ANOVA) with Bonferroni or Newman–Keuls correction for multiple comparisons. Probability values of less than 0.05 were considered significant and tests were performed two-sided. Data was tested for outliers using the Grubbs outlier test and, if outliers were present, they were removed. Data are presented as mean.

Full Methods and any associated references are available in the online version of the paper.

Received 13 April 2011; accepted 16 January 2013.
Published online 20 February 2013.

1. Lakatta, E. G. Age-associated cardiovascular changes in health: impact on cardiovascular disease in older persons. *Heart Fail. Rev.* **7,** 29–49 (2002).
2. Wellenius, G. A. & Mittleman, M. A. Disparities in myocardial infarction case fatality rates among the elderly: the 20-year Medicare experience. *Am. Heart J.* **156,** 483–490 (2008).
3. Small, E. M. & Olson, E. N. Pervasive roles of microRNAs in cardiovascular biology. *Nature*, **469,** 336–342 (2011).
4. Dimmeler, S. & Nicotera, P. MicroRNAs in age-related diseases. *EMBO Mol. Med.* http://dx.doi.org/10.1002/emmm.201201986 (22 January 2013).
5. Thum, T. *et al.* MicroRNA-21 contributes to myocardial disease by stimulating MAP kinase signalling in fibroblasts. *Nature* **456,** 980–984 (2008).
6. van Rooij, E. *et al.* Dysregulation of microRNAs after myocardial infarction reveals a role of miR-29 in cardiac fibrosis. *Proc. Natl Acad. Sci. USA* **105,** 13027–13032 (2008).
7. Christoffersen, N. R. *et al.* p53-independent upregulation of miR-34a during oncogene-induced senescence represses MYC. *Cell Death Differ.* **17,** 236–245 (2010).
8. Boon, R. A. *et al.* MicroRNA-29 in aortic dilation: implications for aneurysm formation. *Circ. Res.* **109,** 1115–1119 (2011).
9. van Almen, G. C. *et al.* MicroRNA-18 and microRNA-19 regulate CTGF and TSP-1 expression in age-related heart failure. *Aging Cell* **10,** 769–779 (2011).
10. He, L. *et al.* A microRNA component of the p53 tumour suppressor network. *Nature* **447,** 1130–1134 (2007).
11. Hermeking, H. MicroRNAs in the p53 network: micromanagement of tumour suppression. *Nature Rev. Cancer* **12,** 613–626 (2012).
12. Krützfeldt, J. *et al.* Silencing of microRNAs *in vivo* with 'antagomirs'. *Nature* **438,** 685–689 (2005).
13. Ito, T., Yagi, S. & Yamakuchi, M. MicroRNA-34a regulation of endothelial senescence. *Biochem. Biophys. Res. Commun.* **398,** 735–740 (2010).
14. Zhao, T., Li, J. & Chen, A. F. MicroRNA-34a induces endothelial progenitor cell senescence and impedes its angiogenesis via suppressing silent information regulator 1. *Am. J. Physiol. Endocrinol. Metab.* **299,** E110–E116 (2010).
15. Xu, Q. *et al.* Micro-RNA-34a contributes to the impaired function of bone marrow-derived mononuclear cells from patients with cardiovascular disease. *J. Am. Coll. Cardiol.* **59,** 2107–2117 (2012).
16. De Leon, G., Sherry, T. C. & Krucher, N. A. Reduced expression of PNUTS leads to activation of Rb-phosphatase and caspase-mediated apoptosis. *Cancer Biol. Ther.* **7,** 833–841 (2008).
17. Kim, H. *et al.* TRF2 functions as a protein hub and regulates telomere maintenance by recognizing specific peptide motifs. *Nature Struct. Mol. Biol.* **16,** 372–379 (2009).
18. Landsverk, H. B. *et al.* The protein phosphatase 1 regulator PNUTS is a new component of the DNA damage response. *EMBO Rep.* **11,** 868–875 (2010).
19. Karlseder, J., Broccoli, D., Dai, Y., Hardy, S. & de Lange, T. p53- and ATM-dependent apoptosis induced by telomeres lacking TRF2. *Science* **283,** 1321–1325 (1999).
20. Sahin, E. *et al.* Telomere dysfunction induces metabolic and mitochondrial compromise. *Nature* **470,** 359–365 (2011).
21. Shukla, P. C. *et al.* BRCA1 is an essential regulator of heart function and survival following myocardial infarction. *Nature Commun.* **2,** 593 (2011).
22. Oh, H. *et al.* Telomere attrition and Chk2 activation in human heart failure. *Proc. Natl Acad. Sci. USA* **100,** 5378–5383 (2003).
23. Yamakuchi, M., Ferlito, M. & Lowenstein, C. J. miR-34a repression of SIRT1 regulates apoptosis. *Proc. Natl Acad. Sci. USA* **105,** 13421–13426 (2008).
24. Hsu, C. P. *et al.* Silent information regulator 1 protects the heart from ischemia/reperfusion. *Circulation* **122,** 2170–2182 (2010).
25. Bernardo, B. C. *et al.* Therapeutic inhibition of the miR-34 family attenuates pathological cardiac remodeling and improves heart function. *Proc. Natl Acad. Sci. USA* **109,** 17615–17620 (2012).
26. Bonauer, A. *et al.* MicroRNA-92a controls angiogenesis and functional recovery of ischemic tissues in mice. *Science* **324,** 1710–1713 (2009).

Supplementary Information is available in the online version of the paper.

Acknowledgements We thank M. Muhly-Reinholz, A. Knau, B. Zimmermann, N. Reinfeld and F. Gehring for technical assistance, F. W. Alt for providing SIRT1 mutant mice and D. Sassoon and G. Marazzi for conceptual advice. R.A.B. was supported by the Netherlands Organization for Scientific Research (NWO) and K.I. by a Research Grant Abroad of the Japanese Heart Foundation. This study was supported by a start-up grant of the Excellence Cluster Cardiopulmonary System (Exc 147-1) to R.A.B., by the European Research Council (Advanced grant ''Angiomirs'') and the German Center for Cardiovascular Research DZHK and the European Union FP7 project Endostem (Grant no. 241440) to S.D. H.A.K. and O.J.M. are supported by the German Centre for Cardiovascular Research (DZHK) and by the German Ministry of Education and Research (BMBF). M.P. is supported by the Max Planck Society, the Fondation Leducq (ARTEMIS) and an ERC Starting Grant (ANGIOMET). H.H. is supported by the DFG, the Deutsche Krebshilfe and the Rudolf-Bartling-Stiftung.

Author Contributions R.A.B. designed and performed experiments, analysed data and wrote the manuscript. S.L. and H.H. generated the *miR-34a*$^{-/-}$ mice. K.I., T.S., A.F., S.H., D.K., K.T., G.C. and A.B. performed experiments and analysed data. A.J.G.H. analysed microarray data. N.D., Z.G., P.B., J.R.E. and M.P. provided essential materials. H.A.K. and O.J.M. developed the AAV vectors. A.M.Z. wrote the manuscript. S.D. designed experiments, analysed data and wrote the manuscript. All authors have proofread the manuscript.

Author Information Data are available at the National Center for Biotechnology Information Gene Expression Omnibus (GEO) and are accessible through GEO Series accession number GSE43556. Reprints and permissions information is available at www.nature.com/reprints. The authors declare competing financial interests: details accompany the full-text HTML version of the paper at www.nature.com/nature. Readers are welcome to comment on the online version of the paper. Correspondence and requests for materials should be addressed to S.D. (dimmeler@em.uni-frankfurt.de).

©2013 Macmillan Publishers Limited. All rights reserved

METHODS

Laboratory animals, ethics and acute myocardial infarction model. C57BL/6 mice were obtained from Charles River and Janvier. *Sirt1*$^{+/-}$ mice[27] and *Ku80*$^{-/-}$ mice were described previously[28]. *miR-34a*$^{-/-}$ mice (SV/C57Bl6 background) were generated using homologous recombination with a vector containing *miR-34a* seed flanked with *loxP* sites and an intronic neomycin resistance (*Neo*) cassette flanked by *frt* sites. The *Neo* cassette was removed by crossing to *flp*-mice and *miR-34a* by crossing with CMV-Cre-mice. As a control, mice homozygous for *miR-34a* flanked with *loxP* sites were used. Generation of *miR-34a*$^{-/-}$ mice will be described in detail elsewhere (Hermeking *et al.*, in preparation). *miR-34a*$^{-/-}$ mice showed no obvious phenotype and were born at normal Mendelian ratio. The animal experiments were approved by the Regional Board of the State of Hessen, Germany. Patient material was obtained under informed consent and according to the declaration of Helsinki. Acute myocardial infarction operations were performed as described[26] and the mice were subsequently evaluated to assess the infarct size, after which mice received treatment. Echocardiography was performed using a Vevo-770 (Visualsonics) by a researcher blinded to the experimental conditions. Antagomirs (8 mg kg^{-1}) were synthesized by VBC Biotech as described previously[26]. The following sequences were used in this study: Ant-Control: 5′-AAGGCAAGCUGACCCUGAAGUU-3′ and Ant-34a: 5′-ACAACCAGCUAAGACACUGCCA-3′. LNA-Anti-miRs (LNA/DNA mixmers) (20 mg kg^{-1} in *Ku80*$^{-/-}$ mice and 5 mg kg^{-1} in wild-type mice) were from Exiqon and the sequences were LNA-Control: 5′-ACGTCTATACGCCCA-3′, T_m 75 °C; and LNA-34a: 5′-AGCTAAGACACTGCC-3′, T_m 74 °C.

Cell culture, transfection and flow cytometry. Rat neonatal cardiomyocyte isolation was performed as described[29]. Human (GATA-4$^+$/α-sarcomeric actin$^+$) cardiomyocytes were purchased from Promocell. Separation of mouse cardiomyocytes and non-cardiomyocytes using Langendorff-perfusion-mediated digestion was performed as described[26]. Transfection of cardiomyocytes with pre-miR constructs (pre-miR-34a: 5′-GGCCAGCUGUGAGUGUUUCUUUGGCAGUGUCUUAGCUGGUUGUUGUGAGCAAUAGUAAGGAAGCAAUCAGCAAGUAUACUGCCCUAGAAGUGCUGCACGUUGUGGGGCCC-3′; pre-miR-control: Pre-miR Negative Control #1 from Life Technologies) and anti-miR hairpin inhibitors (miRIDIAN microRNA hsa-mir-34a hairpin inhibitor and miRIDIAN microRNA Hairpin Inhibitor Negative Control #1 from Thermo Fischer), both at 30 nM, as well as siRNA (mix of two sequences targeting *Trf2* (5′-CCCAAAGUACCCAAAGGCA-3′ and 5′-GCUUCAGCGCCACCAUCCA-3′, 20 nM each) or one negative control siRNA (5′-CGUACGCGGAAUACUUCGA-3′, 40 nM)) transfection was performed using HiPerfect reagent (Qiagen). Apoptosis was quantified using annexin V and 7-AAD staining and flow cytometry analysis using a CantoII (BD Biosciences). Annexin V-positive/7-AAD-negative cell populations were considered apoptotic.

RNA isolation, real-time PCR and transcriptional profiling. Total RNA isolation was performed with miRNeasy kits from Qiagen and real-time PCR with Applied Biosystems microRNA assays run on an Applied Biosystems StepOnePlus. miRNA levels were normalized with *Rnu6* and *Sno202* expression and mRNA levels with *Rplp0*. Quantification of real-time PCR was performed using synthetic microRNA sequences in a calibration curve. Transcriptional profiling was performed by DNAvision on the Agilent-v1 platform (570 miRNAs) or on the Affymetrix 430 v2.0 platform (mRNA, full genome). Data was background-corrected and normalized by quantile normalization. Statistical comparisons were done using a Bayesian one-way ANOVA and probability values were corrected for multiple testing with the Benjamini–Hochberg false discovery rate method[30]. Data are available at the National Center for Biotechnology Information Gene Expression Omnibus (GEO) and are accessible through GEO Series accession number GSE43556.

Microscopy, microRNA *in situ* hybridization, telomere assays and histology. Confocal microscopy and *in situ* hybridization was performed as described before[26], with the following modifications: miR-34a LNA-modified detection probe (5′ and 3′ DIG-labelled) was from Exiqon, hybridization temperature 57 °C. Telomere length was measured using real-time PCR, as described before[31], as well as by quantitative fluorescence *in situ* hybridization (Q-FISH), using the telomere PNA FISH Cy3 kit (Dako). Chromosome spreads were generated by addition of Colcemid (0.1 μg ml^{-1}, 24 h) and after hybridization, images were captured with a Zeiss Axio Observer and ×63 objective. Telomere signals were quantified with TFL-Telo in a blinded manner[32]. Green fluorescent microspheres (Invitrogen) were used to normalize between slides. Telomerase activity was measured with the TRAPeze ELISA telomerase kit (Millipore). TUNEL (cell death) and Sirius red (fibrosis) staining was performed as described[26]. Fibrosis in infarcted hearts was quantified as described[33].

Luciferase assays, lentivirus, AAV and western blotting. Luciferase constructs were made by inserting the full-length human *PNUTS* 3′UTR, obtained from Imagenes in the psiCheck2 vector (Promega), in which the putative miR-34a seed sequence binding site (5′-CACTGCC-3′) was mutated to 5′-CTGTCGC-3′. Smaller UTR fragments were inserted using the following oligos: 2x-miR-34a: 5′-aagtcacactacatgcactgcctttgaaagtcacactacatgcactgcctt-3′, 2x-miR-34a-mut: 5′-aagCTacacATcatgcTGtCGctttgaaagCTacacATcatgcTGtCGctt-3′, miR-34a-footprint: 5′-tgctgggcctgaaagtcacactacatgcactgcctttgggagtcagctcactccctgctcc-3′, mut-footprint: 5′-tgctgggcctgaaagCTacacATcatgcTGtCGctttgggagtcagctcactccctgctcc-3′. Mutations are highlighted as uppercase. psiCheck2 plasmids were transfected in HEK293T cells using Genejuice (Merck) and pre-miR-34a and control RNA (Applied Biosystems), as well as LNA-Control and LNA-34a were transfected using Ribojuice (Merck). PNUTS cDNA was obtained in pDONR221 (Imagenes) and shuttled to the pLenti4 vector (Invitrogen). Lentiviral particles were generated as described[34]. Western blotting was carried out as described[26]. For adeno-associated virus vector generation, *PNUTS* complementary DNA flanked by BamHI and Xba1 restriction sites was inserted into pUF-CMV/MLC0.26, a derivate of pUF-CMV/MLC0.26-μDys[35]. An AAV vector genome containing *Renilla* luciferase under control of the CMV/MLC0.26 promoter was used as control. AAV9 vectors were generated and titrated as described before[35,36]. Mice received 7×10^{11} vector genomes. Anti-PNUTS antibodies were from R&D Systems, anti-γ-H2A.X, anti-P-CHK2 and anti-CHK2 antibodies were from Cell Signaling.

Statistical analysis. Data were analysed with GraphPad Prism 5 using student's *t*-tests when comparing two conditions, or an ANOVA with Bonferroni or Newman–Keuls correction for multiple comparisons. Probability values of less than 0.05 were considered significant and tests were performed two-sided. Data was tested for outliers using the Grubbs outlier test and, if outliers were present, they were removed. Data are presented as mean and error bars depict the standard error of the mean (s.e.m.).

27. Cheng, H. L. *et al.* Developmental defects and p53 hyperacetylation in Sir2 homolog (SIRT1)-deficient mice. *Proc. Natl Acad. Sci. USA* **100,** 10794–10799 (2003).
28. Vogel, H., Lim, D.-S., Karsenty, G., Finegold, M. & Hasty, P. Deletion of Ku86 causes early onset of senescence in mice. *Proc. Natl Acad. Sci. USA* **96,** 10770–10775 (1999).
29. Koyanagi, M., Brandes, R. P., Haendeler, J., Zeiher, A. M. & Dimmeler, S. Cell-to-Cell Connection of Endothelial Progenitor Cells With Cardiac Myocytes by Nanotubes: A Novel Mechanism for Cell Fate Changes? *Circ. Res.* **96,** 1039–1041 (2005).
30. Reiner, A., Yekutieli, D. & Benjamini, Y. Identifying differentially expressed genes using false discovery rate controlling procedures. *Bioinformatics* **19,** 368–375 (2003).
31. Cawthon, R. M. Telomere measurement by quantitative PCR. *Nucleic Acids Res.* **30,** e47 (2002).
32. Poon, S. S. S., Martens, U. M., Ward, R. K. & Lansdorp, P. M. Telomere length measurements using digital fluorescence microscopy. *Cytometry* **36,** 267–278 (1999).
33. Takagawa, J. *et al.* Myocardial infarct size measurement in the mouse chronic infarction model: comparison of area- and length-based approaches. *J. Appl. Physiol.* **102,** 2104–2111 (2007).
34. Boon, R. A. *et al.* Kruppel-like factor 2 improves neovascularization capacity of aged proangiogenic cells. *Eur. Heart J.* **32,** 371–377 (2011).
35. Schinkel, S. *et al.* Long-term preservation of cardiac structure and function after adeno-associated virus serotype 9-mediated microdystrophin gene transfer in *mdx* mice. *Hum. Gene Ther.* **23,** 566–575 (2012).
36. Hauswirth, W. W., Lewin, A. S., Zolotukhin, S. & Muzyczka, N. Production and purification of recombinant adeno-associated virus. *Methods Enzymol.* **316,** 743–761 (2000).

©2013 Macmillan Publishers Limited. All rights reserved